JOURNAL OF COMPUTATIONAL
AND THEORETICAL NANOSCIENCE
Vol. 1. 29–40, 2004

Multi-scale Modeling of Si and C Nanocluster Nucleation During Non-equilibrium Gas Phase Processing

Gregory A. Johnson* and Nasr M. Ghoniem

Mechanical and Aerospace Engineering Department, University of California, Los Angeles, California 90095-1597, USA

Methods of developing nanophase materials of controlled and uniform size distribution are critical to many emerging electronic and mechanical applications. The objective of this work is to develop a hierarchy of models, based on quantum chemistry, statistical mechanics and the theory of rate processes, to enable a complete description of the nucleation and growth of nanoclusters of controlled size distributions. The model is applied to the process of nanocluster nucleation in expanding plasma or combustion nozzles. The energetics of Si and C clusters containing up to 10 atoms are developed using ab initio and semi-empirical quantum mechanics. Rate constants are then obtained for determining Si clustering rates. The results of these calculations compare well with published experimental data.

Keywords: Carbon, Nanoclusters, Nucleation, Plasma, Quantum Chemistry, Silicon, Statistical Mechanics.

RESEARCH ARTICLE

1. INTRODUCTION

Nanoclusters are manufactured by various techniques, including organic precursor-based synthetic chemistry, aqueous colloidal processing, low temperature thermalization of organorare-earth clusters, metallo-organic pyrolysis,[1] and laser ablation of different materials.[2] All of these synthesis techniques rely upon cluster growth mechanisms, which are controlled by the chemistry of participating species. Chemical techniques are used for producing semiconductor nanocrystals, for example, and are generally accompanied by the formation of unanticipated by products.[3] Furthermore, the chemical sensitivity toward oxidation or reducibility of chemical constituents, plus the necessary care in the choice of anion or cation precursor components, greatly impact control of nanocrystal production. Chemical reaction rates, or limited availability of suitable chemical precursors, can limit the composition, type and size[4] of nanoparticles and nanoparticle-based structures that can be obtained. When hot gas processing is considered as a route to nanocluster manufacturing, additional degrees of freedom become available to control nanoparticle formation and deposition. Independent control of the precursor densities, gas temperature, precursor saturation ratio (i.e., supersaturation) and many other parameters is possible in a hot gas environment. The flexibility of this technique allows it to be used for making bulk material, thin films and coatings. In addition, the ability to produce and sustain a non-equilibrium state to drive the desired hot gas chemistry or reaction rates provides many new possibilities for scientists to explore and understand the fabrication and manipulation of nanoparticles. Because of the large number of hot gas process variables, however, an accurate model for the evolution of cluster size distribution is needed.

Most nanophase materials are 100 nm or less in size and contain fewer than tens of thousands of atoms. Conventional materials, on the other hand, consist of grains ranging from microns to millimeters, and contain several billion atoms. The small size of the grains and the grain size distribution are what give nanophase materials their unique properties, many of which are still under investigation. The key in practical utilization of nanophase materials is accurate control of the grain size and size distribution, allowing the properties of the material to be tailored for a specific requirement. Theoretical methods for accurately determining the properties of nanophase materials based on their size

*Author to whom correspondence should be addressed.

distribution are needed to predict properties before the materials are produced.

The primary focus of this paper is to present a model that describes the nucleation, formation and evolution of the cluster size distribution of nanophase carbon and silicon within a hot gas environment. The objective is to explore methods that enable control of the cluster size distribution, and to eliminate the characteristic tail as a result of competition between nucleation of small size clusters and growth of larger ones. This tail is characteristic of all experimental results to date (see, for example, Reference 5). The goal of this research is to develop a computational multiscale framework to model and design non-equilibrium gas phase synthesis experiments. With this model, investigations of the effects of experimental design variables such as quench rate, temperature, supersaturation and other parameters of interest on the cluster size distribution can be carried out.

2. CLUSTER NUCLEATION MODEL

Current approaches to modeling the formation of nanoclusters are based on classical nucleation theory. Isolated atoms or molecules combine to form embryos, which are unstable until a critical size is reached. The vapor pressure and surface tension of the material at the temperature and supersaturation of interest determine the critical size for nucleation.[6–8] This approach is not adequate, because the calculated nucleation rate is very sensitive to the exact values of the surface tension and degree of vapor supersaturation. Because the properties of nanophase materials are fundamentally different from bulk properties, the classical approach of using phenomenological parameters based on bulk properties to describe sequential nucleation and growth of very small particles is questionable. In the following, we present a more fundamental approach to modeling the evolution of nanoclusters in supersaturated vapors, and apply it to the conditions of nucleation within a hot gas environment. Quantum mechanics is used to determine cluster energetics for cluster sizes up to 10 atoms. With this information, rate constants are determined. Quantum-Rice-Ramsperger-Kassel (QRRK) theory,[9–16] augmented by Transition State Theory[6, 9, 10] and Collision Rate Theory,[6, 7, 11] are used to determine the rate constants for clustering reactions. Once this information is in hand, rate equations can be determined, and the evolution of the size distribution studied.

2.1. Quantum Chemistry of Clusters

The objective of performing quantum mechanical calculations is to determine, with great accuracy, a number of parameters that are needed for further rate constant development. These parameters are cluster binding energy, cluster normal modes of vibration and cluster principal moments of inertia. Determination of cluster energetics requires that Schrödinger's equation for the collection of atoms be solved with all the associated nuclei and electrons in three dimensions. For a molecule with N nuclei and n electrons, the time independent Schrödinger equation is given by:[6, 9, 12, 13]

$$H\psi = (T_N + T_e + V_{Ne} + V_{NN})\,\psi = E_T\psi \qquad (1)$$

where H is the Hamiltonian, and T and V are the kinetic and potential energy operators, respectively. The subscripts N and e refer to nuclear and electronic components, respectively. Most modern approaches rely on the implementation of the Born-Oppenheimer (BO) approximation.[9, 12, 13] Because the nuclei are much more massive than the electrons, they are assumed to be stationary. Henceforth, the kinetic energy of nuclei is ignored, allowing separation of the total wave function into a product of the electronic (ψ_{elec}) and nuclear (ψ_{nuc}) wave functions.

The energetics of silicon and carbon clusters of sizes up to 10 atoms have been calculated using the General Atomic and Molecular Electronic Structure System (GAMESS) software package.[14] This was accomplished by utilizing the built-in geometry optimizer that locates relative potential energy minima. Because a given cluster may contain several local minima, numerous initial conditions were tried in order to ascertain that the final configuration is an absolute minimum. Calculations were performed using both ab initio and semi-empirical methods. In the former, the BO approximation and linear combination of atomic orbitals (LCAO) molecular orbital (MO) theory for each electron in the system are utilized. Semi-empirical methods, on the other hand, are based on neglecting differential overlap (NDO) of inner electrons.[15] Calculations were performed with the two methods for silicon clusters, and with the ab initio method only for carbon clusters. The basis sets (e.g., sets of atomic orbitals) used were the TZV[16] basis set for the ab initio calculations and the PM3[17] basis set for the semi-empirical calculations. In this manner, cluster binding energy, configuration and normal modes of vibration were determined. This information is subsequently used to evaluate the rate constants, which are necessary to describe nucleation and clustering.

For small size clusters, binding energies determined from quantum mechanics calculations were directly used in subsequent rate calculations. For larger clusters, however, the binding energy as a function of cluster size was appropriately extrapolated. The method used was a modified version of the capillary model. The unmodified capillary model is given as:

$$E_{binding} = m\phi x\,(1 - ax^{-1/3}) \qquad (2)$$

Here, $E_{binding}$ is the total cluster binding energy, m is the number of bonds per atom, ϕ is the energy per bond and x is the number of atoms in the cluster. The parameter a is a surface parameter which serves as a proportionality constant for the number of surface atoms per bulk atom, and accounts for the average number of bonds a surface atom is

deficient with respect to a bulk atom. The energy per bond is related to the heat of sublimation at 0 K by:

$$\phi = \frac{\Delta H_{sublimation}}{m} \tag{3}$$

The modified version of the capillary we propose is given as:

$$E_{binding} = m\phi x\,(1 - x^{\alpha})(1 - ax^{-1/3}) \tag{4}$$

Here a power law factor, $(1 - x^{\alpha})$, has been added to provide a better fit to the quantum mechanics data for small size clusters, where α is determined empirically.

2.2. Cluster Reaction Rates

As previously mentioned, QRRK theory, augmented with Transition State Theory and Collision rate theory, is used to determine rate constants. QRRK theory was originally developed to explain unimolecular reactions. Later refinements allow its use for bimolecular reactions. The underlying inherent assumptions are the following:

1. Each cluster consists of S oscillators, where $S = 3i - 6$ ($S = 3i - 5$ for linear clusters), where i is the number of atoms within the cluster.
2. Each oscillator has the same fundamental frequency, ν.
3. The vibrational energy is quantized.
4. The critical oscillator (where bonds are broken/formed) must contain at least m_{crit} quanta, where $m_{crit} = \varepsilon_0/h\nu$, for a reaction to occur.
5. Clusters gain/lose vibrational energy by collisions with the surrounding bath gas.
6. Statistical redistribution occurs at each collision; and the concentration of clusters in each energized state (containing sufficient vibrational energy to react) is maintained at steady state.

Using silicon as an example, the dissociation mechanism is given as:

$$\begin{aligned} Si_{i+j} + M &\xrightarrow{k_1} Si^*_{i+j} + M \\ Si^*_{i+j} + M &\xrightarrow{k_2} Si_{i+j} + M \\ Si^*_{i+j} &\xrightarrow{k_3} Si_i + Si_j \end{aligned} \tag{5}$$

where the first reaction is the rate at which clusters of size $i + j$ are energized to state n; the second reaction is the rate at which these energized clusters are knocked out of state n to a different state; and the third reaction is the rate at which these energized clusters dissociate into clusters of size i and size j. The distribution of vibrational quanta in a cluster is given as:[18, 19]

$$P_n = \frac{(n+s-1)!}{n!(s-1)!} e^{-n\beta h\nu}(1 - e^{-\beta h\nu})^s \tag{6}$$

where n *is* the number of quanta, s is the number of vibrational modes, $\beta = 1/kT$, h is Planck's constant and ν is the vibrational frequency. The collision rate constant, k_2, at which clusters in vibrational state n are knocked out of this state is given as:[11]

$$k_2 = \sigma\sqrt{\frac{8kT}{\pi\mu}} \tag{7}$$

where σ is the collision cross-section, k *is* Boltzmann's constant, and μ is the reduced mass of the collision pair. The rate constant, k_1, at which clusters are knocked into vibrational state n is:[18]

$$k_1 = k_2 P_n \tag{8}$$

The rate constant, k_3, at which energized clusters in vibrational state n dissociate is:[18, 19]

$$k_3(n) = A\frac{n!(n - m_{crit} + s - 1)!}{(n - m_{crit})!(n + s - 1)!} \tag{9}$$

where it has been noted that k_3 is a function of n. Applying the constrained equilibrium approximation to the excited clusters in vibrational state n gives:

$$k_1[Si_{i+j}][M] = k_2[Si^*_{i+j}][M] + k_3[Si^*_{i+j}] \tag{10}$$

which upon rearrangement and use of Equation 8, gives:

$$[Si^*_{i+j}] = \frac{P_n[Si_{i+j}]}{1 + k_3/k_2[M]} \tag{11}$$

Now the rate of dissociation is $k_3(n)[Si^*_{i+j}]$. Inserting Equation 11 and summing over all energized states, one obtains:

$$k_{diss} = \sum_{n=m_{crit}}^{\infty} \frac{k_3(n)P_n}{1 + k_3(n)/k_2[M]} \tag{12}$$

Using Equations 6, 7 and 9 and substituting $p = n - m_{crit}$ into Equation 12, the final result is:[18]

$$k_{diss}(i + j \rightarrow i, j) = Ae^{-\beta\varepsilon_0}(1 - e^{-\beta h\nu})^s \sum_{p=0}^{\infty} \frac{\dfrac{(p+s-1)!}{p!(s-1)!}e^{-p\beta h\nu}}{1 + \dfrac{A\dfrac{(p+m_{crit})!(p+s-1)!}{p!(p+m_{crit}+s-1)!}}{\sigma\sqrt{8kT/\pi\mu[M]}}} \tag{13}$$

At high pressures (i.e., large values of [M]), Equation 13 becomes:[18, 19]

$$k_{diss}(i + j \rightarrow i, j) = Ae^{-\beta\varepsilon_0} \tag{14}$$

By constraining the maximum rate constant to that predicted by Transition State Theory,[10] the parameter A can be determined to be:

$$A = \left(\frac{kT}{h}\right)\frac{q^{\ddagger}_{i+j}}{q_{i+j}} \tag{15}$$

RESEARCH ARTICLE

where $q^{\ddagger}_{i+j}$ is the partition function of the activated complex (e.g., Transition State) and q_{i+j} is the partition function of the cluster.

The mechanism for recombination is given as:

$$\begin{aligned} Si_i + Si_j &\xrightarrow{k_4} Si^*_{i+j} \\ Si^*_{i+j} &\xrightarrow{k_3} Si_i + Si_j \\ Si^*_{i+j} + M &\xrightarrow{k_2} Si^*_{i+j} + M \end{aligned} \tag{16}$$

where the first reaction is the rate of recombination of size i and j clusters to form an energized cluster of size $i + j$ in energized state n. The second reaction is the rate at which energized clusters of size $i + j$ decompose into clusters of size i and j. The last reaction is the rate at which these energized clusters are knocked into a different state. By similar arguments used to develop the dissociation rate constant and by applying the principle of detailed balance,[20] the recombination rate constant can be shown to be:

$$k_{rec}(i, j \rightarrow i + j) = A'(1 - e^{-\beta h\nu})^s \sum_{p=0}^{\infty} \frac{\dfrac{(p+s-1)!}{p!(s-1)!} e^{-p\beta h\nu}}{1 + \dfrac{A}{\sigma\sqrt{8kT/\pi\mu[M]}} \dfrac{(p+m_{crit})!(p+s-1)!}{p!(p+m_{crit}+s-1)!}} \tag{17}$$

where now:

$$A' = \left(\frac{kT}{h}\right)\frac{q^*_{i+j}}{q_i q_j} \tag{18}$$

The next step is to calculate the rate constants to be used in the coupled set of ordinary differential equations. For cluster sizes of 10 atoms and less, the information obtained from the ab initio calculations was used to determine the rate constants. The average frequency was determined by using the Einstein model for the heat capacity of a solid, as follows:

$$s(\beta h\bar{\nu})^2\left[\frac{e^{-\beta h\bar{\nu}}}{(e^{-\beta h\bar{\nu}} - 1)^2}\right] = \sum_{j=1}^{s} (\beta h\nu_j)^2\left[\frac{e^{-\beta h\nu_j}}{(e^{-\beta h\nu_j} - 1)^2}\right] \tag{19}$$

For larger size clusters, the information required to determine the rate constants was extrapolated from the ab initio calculations or inferred from other physical data. For example, the binding energy was extrapolated using the modified capillary model previously mentioned. The principal moments of inertia, required for computing the rotational partition function, was determined by assuming a spherical shape and using the density of the bulk solid; for the transition states, two spheres of size i and j are assumed and the parallel axis theorem is used.[21] A detailed study of the silicon dimer reaction indicates that the rotational energy barrier occurs at a separation distance of around 9 Å.[22] This distance was used to determine the moments of inertia of the transition state. Also needed is the rotational symmetry. Rotational symmetry is the number of distinct rotations that produce indistinguishable configurations. From ab initio calculations, the rotational symmetry is known for clusters up to size 10. It is also known that bulk silicon crystal has a rotational symmetry number of 36.[23] Reaction degeneracy—the number of channels available for a reaction to occur (e.g., the reaction $CH_4 \rightarrow CH_3 + H$ has reaction degeneracy of 4)—is accounted for by rotational symmetry numbers. For small size clusters, no modifications are necessary. The reaction degeneracy is properly taken into account by the rotational symmetries. For large size clusters, however, the maximum rotational symmetry is 36 for crystalline silicon. This would imply that the maximum number of sites available for monomer evaporation from a large size cluster would be 36. But this seems unreasonable since all surface atoms are essentially the same. Therefore, a correction is needed to account for the expected increased degeneracy. An exponential function was proposed because it rapidly approaches the expected degeneracy. This equation is

$$\sigma_{rot_{psuedo}} = \sigma_a + \frac{4\pi}{\sqrt{3}}\left(\frac{3i}{4\pi}\right)^{2/3}(1 - e^{-\lambda_{rot} i}) \tag{20}$$

where, for silicon,

$\sigma_{rot_{pseudo}}$ is the cluster psuedo rotational symmetry number
σ_a = 1.85
λ_{rot} = 0.008
i is the number of atoms in the cluster

The average oscillator frequency was determined using the Einstein model for the heat capacity of a solid, but this time finding the Einstein frequency which agreed well with published heat capacity data.[24] Finally, the collision cross-section between the excited cluster Si^*_{i+j}, and the bath gas M, is needed to determine the de-energization rate constant k_2. The hard sphere model is used where the radius of the cluster is given by

$$r_{i+j} = \sqrt[3]{\frac{3\Omega}{4\pi}(i+j)} \tag{21}$$

where Ω is the atomic volume, and the radius of the bath gas M is obtained from the literature.[25] The parameters used in the model presented herein to calculate the dissociation and recombination rate constants for silicon are summarized in Table 1.

Table 1. Input parameters to rate constant equations

Parameter	Used in	Value
m	Equation 4	2.0
$\phi(eV)$	Equation 4	2.3095
α	Equation 4	−0.13852
$\nu\ (cm^{-1})$	Equations 13, 15, 17 & 18	309.487
σ_a	Equation 20	1.85
λ_{rot}	Equation 20	0.008
σ_{Ar} (Å)	Equations 7, 13 & 17	6.459

2.3. Rate Equations for Cluster Evolution

Now that the rate constants are available, the time-dependent nature of nucleation and clustering can be studied. The time-dependent cluster equation is given as:

$$dC_i/dt = \frac{1}{2}\sum_{j=1}^{i-1}[K_{rec}(j,i-j)C_jC_{i-j} - (1-\delta_{j,i-j})K_{diss}(j,i-j)C_i] + \sum_{j=1}^{\infty}[(1+\delta_{i,j})K_{diss}(i,j)C_{i+j} - K_{rec}(i,j)C_iC_j] + S_i \quad (22)$$

where the first term is the recombination rate of clusters of size j and $i-j$ to form clusters of size i. The second term is the dissociation rate of clusters of size i into clusters of size j and $i-j$. The third term is for the dissociation rate of clusters of size $i+j$ into clusters of size i and j. The fourth term is for the recombination rate of clusters of size i and j into clusters of size $i+j$. And the last term is a source term which is usually the rate of monomer introduction for $i=1$ and zero for cluster sizes greater than 1. Equation 22 is a coupled set of stiff, initial value, ordinary differential equations. Solutions of this set of differential equations gives the time-dependent nature of the cluster size distribution. Unfortunately, in order to include the size range of interest in the model, it would require an unrealistic number of equations. For instance, a 10 *nm* silicon particle contains about 30,000 monomers and a 100 *mm* silicon particle contains about 30,000,000 monomers. Thus, to include 100 *nm* sized particles would require 30,000,000 equations. For this reason, two approximation techniques are introduced to greatly reduce the number of equations to be solved. These are the discrete sectional method and the moments method.

2.3.1. Discrete Sectional Method

The discrete sectional method tackles the problem of the large size domain by dividing the domain into sections.[26] Each section consists of a large portion of the size domain. All particles in a section take on the sectional average properties. This greatly reduces the number of conservation equations. Typically, the size domain is divided into several (10–30) equal logarithmic sections. Development of the discrete sectional method is as follows.

Multiplying Equation 22 by i^k and summing over all i, gives[27, 28]

$$dN_k/dt = \frac{1}{2}\sum_{i=1}^{\infty}\sum_{j=1}^{\infty}[K_{rec}(i,j)C_iC_j - (1-\delta_{i,j})K_d(i,j)C_{i+j}] \times[(i+j)^k - i^k - j^k] + \sum_{i=1}^{\infty} i^k S_i \quad (23)$$

where the moments of the cluster size distribution are defined as

$$N_k(t) = \sum_{i=1}^{\infty} i^k C_i(t) \quad (24)$$

For $k=1$, Equation 23 becomes

$$dN_1/dt = \frac{1}{2}\sum_{i=1}^{\infty}\sum_{j=1}^{\infty}[K_{rec}(i,j)C_iC_j - (1+\delta_{i,j})K_d(i,j)C_{i+j}] \times[(i+j)-i-j] + \sum_{i=1}^{\infty} iS_i \quad (25)$$

which is a conservation equation for the number of monomers in the system. The flux of monomers, Q, into section l due to recombination reactions is

$$Q_{m+n\to l} = \frac{1}{2}\sum_{i=\max[(k_l+1-(k_n+1)),(k_m+1)]}^{\min\{[k_l+1-(k_n+1)],k_m+1\}} \sum_{j=\max(k_n+1,\,k_{l+1}+1-i)}^{\min(k_n+1,k_{l+1}-1)} (i+j)K_{rec}(i,j)C_iC_j \quad (26)$$

The flux of monomers, Q, out of section l due to recombination reactions of particles in section l with those in lower sections is

$$Q_{m+l\to n} = -\sum_{i=\max[(k_n+1-(k_l+1)),(k_m+1)]}^{\min\{[k_n+1-(k_l+1)],k_m+1\}} \sum_{j=\max[(k_l+1,k_n+1-i)}^{\min(k_l+1,k_n+1-i)} jK_{rec}(i,j)C_iC_j \quad (27)$$

The flux of monomers, Q, into section l due to recombination of particles in section l with particles in lower sections is

$$Q_{m+l\to l} = \sum_{i=k_{m+1}}^{\min\{[k_l+1-(k_l+1)],k_m+1\}} \sum_{j=k_l+1}^{k_{l+1}-i} iK_{rec}(i,j)C_iC_j \quad (28)$$

The flux of monomers, Q, leaving section l due to recombination of particles in section l is

$$Q_{l+l\to n} = -\frac{1}{2}\sum_{i=\max[(k_n+1-(k_l+1)),(k_l+1)]}^{\min\{[k_n+1-(k_l+1)],k_l+1\}} \sum_{j=\max(k_l+1,k_n+1-i)}^{\min(k_l+1,k_n+1-i)} (i+j)K_{rec}(i,j)C_iC_j \quad (29)$$

RESEARCH ARTICLE

Finally, the flux of monomers, Q, leaving section l due to recombination of particles in section l with particles in higher sections is

$$Q_{l+m\to n} = -\sum_{i=(k_l+1)}^{\min\{[k_{n+1}-(k_m+1)],k_l+1\}} \sum_{j=\max[(k_m+1,\,k_n+1-i)}^{\min(k_{m+1},k_{n+1}-i)} iK_{rec}(i,j)C_iC_j \tag{30}$$

Collecting terms, the conservation of monomers as expressed by the discrete sectional method becomes:

$$dQ_l/dt = [(Q_{m+n\to l} + Q_{m+l\to l}) - (Q_{m+l\to n} + Q_{l+l\to n} + Q_{l+m\to n})] + \sum_{i=k_{l-1}+1}^{k_l} iS_i \tag{31}$$

To express dQ_l/dt in terms of Q_l, so as to obtain a closed set of equations for Q_l, it is necessary to introduce the fundamental approximation inherent in the discrete sectional method. A convenient functional form of the size distribution within the sections must be introduced such that the integral quantity of monomers within the section is equal to Q_l.[26] The simplest functional form is to assume that iC_i is constant within the section. Thus,

$$Q_l = \sum_{k_l}^{k_{l+1}-1} iC_i \tag{32}$$

Defining

$$q_l = iC_i$$

Equation 32 becomes

$$Q_l = q_l\,(k_{l+1} - k_l) \tag{33}$$

Rearrangement then gives

$$C_i = \frac{Q_l}{i(k_{l+1} - k_l)} \tag{34}$$

Equation 34 can then be substituted into Equations 26, 27, 28, 29 and 30, yielding the conservation equation of Q in closed form.

2.3.2. Moments Method

The next approximation method for solving the master equations for the size distribution is the method of moments, or moments method.[27] Starting with the master equations, Equation 22, and the definition of the moments of the size distribution, Equations 23 and 24, we begin by dividing the cluster size domain into two groups: those smaller than x^*, and those larger than x^*. The quantity x^* is some small integer, usually arbitrarily chosen, but may be suggested, in some cases, by the physical properties of the clusters (e.g., their stability). Those cluster sizes smaller than x^* are modeled discretely, and those larger than x^* are modeled as a continuum. For the small size clusters (i.e., $<x^*$), Equation 22 becomes:

$$\begin{aligned} dC_i/dt = {} & \frac{1}{2}\sum_{j=1}^{i-1}[K_{rec}(j,i-j)C_jC_{i-j} - (1+\delta_{j,i-j}) \\ & K_{diss}(j,i-j)C_i] + \sum_{j=i+1}^{x^*}(1+\delta_{i,j-i})K_{diss}(i,j-i)C_j \\ & - \sum_{j=1}^{x^*} K_{rec}(i,j)C_iC_j + \int_{x^*}^{\infty} dx K_{diss}(i,x-i)C_x \\ & - \int_{x^*}^{\infty} dx K_{rec}(i,x)C_iC_x + S_i \end{aligned} \tag{35}$$

And similarly, Equation 23 becomes:

$$\begin{aligned} dN_k/dt = {} & \frac{1}{2}\sum_{i=1}^{x^*}\sum_{j=1}^{x^*}[K_{rec}(i,j)C_iC_j]\times[(i+j)^k - i^k - j^k] \\ & - \frac{1}{2}\sum_{j=2}^{x^*}\sum_{i=1}^{j-1}[(1+\delta_{i,j-i})K_{diss}(i,j-i)C_j] \\ & \times[j^k - i^k - (j-i)^k] \\ & + \sum_{i=1}^{x^*}\int_{x^*}^{\infty} dx[K_{rec}(i,x)C_iC_x]\times[(i+x)^k - i^k - x^k] \\ & - \sum_{i=1}^{x^*-1}\int_{x^*}^{\infty} dx[K_{diss}(i,x-i)C_x]\times[x^k - i^k - (x-i)^k] \\ & + \frac{1}{2}\int_{x^*}^{\infty}\int_{x^*}^{\infty} dxdy[K_{rec}(x,y)C_xC_y]\times[(x+y)^k - x^k - y^k] \\ & - \frac{1}{2}\int_{x^*}^{\infty} dx\int_{x^*}^{\infty} dy[K_{diss}(x,x-y)C_x]\times[x^k - y^k - (x-y)^k] \\ & + \sum_{i=1}^{x^*} i^kS_i + \int_{x^*}^{\infty} dx x^kS(x) \end{aligned} \tag{36}$$

where N_k are the full moments of the size distribution. The moments of the large size cluster distribution are defined as:

$$M_k(t) = \int_{x^*}^{\infty} dx x^kC(x,t) \tag{37}$$

which are related to the full moments approximately by:

$$M_k = N_k - \sum_{i=1}^{x^*} i^kC_i \tag{38}$$

Inserting this into Equation 36 gives, upon rearrangement:

$$\begin{aligned} dM_k/dt = &-\sum_{i=1}^{x^*} i^k dC_i/dt + \sum_{i=1}^{x^*} i^k S_i + \int_{x^*}^{\infty} dx x^k S_x \\ &+ \frac{1}{2}\sum_{i=1}^{x^*}\sum_{j=1}^{x^*}[K_{rec}(i,j)C_iC_j] \times [(i+j)^k - i^k - j^k] \\ &- \frac{1}{2}\sum_{j=2}^{x^*}\sum_{i=1}^{j-1}[(1+\delta_{i,j-i})K_{diss}(i,j-i)C_j] \\ &\times [j^k - i^k - (j-i)^k] \\ &+ \sum_{i=1}^{x^*}\int_{x^*}^{\infty} dx[K_{rec}(i,x)C_iC_x] \times [(i+x)^k - i^k - x^k] \\ &- \sum_{i=1}^{x^*-1}\int_{x^*}^{\infty} dx[K_{diss}(i,x-i)C_x] \times [x^k - i^k - (x-i)^k] \\ &+ \frac{1}{2}\int_{x^*}^{\infty}\int_{x^*}^{\infty} dxdy[K_{rec}(x,y)C_xC_y] \times [(x+y)^k - x^k - y^k] \\ &- \frac{1}{2}\int_{x^*}^{\infty} dx\int_{x^*}^{x} dy[K_{diss}(x,x-y)C_x] \times [x^k - y^k - (x-y)^k] \end{aligned} \quad (39)$$

In general, a function of the sort:

$$G = \int dx g(x) C(x) \quad (40)$$

can be expanded in terms of its moments. Expanding $g(x)$ in a Taylor series expansion gives:

$$\begin{aligned} g(x) &= \sum_{n=0}^{\infty}\frac{1}{n!}g_{x_0}^{(n)}(x-x_0)^n \\ &= \sum_{n=0}^{\infty}\frac{1}{n!}g_{x_0}^{(n)}\sum_{\nu=0}^{n}\binom{n}{\nu}(-x_0)^{n-\nu}x^{\nu} \end{aligned} \quad (41)$$

Inserting Equation 41 into Equation 40 yields:

$$G = \sum_{n=0}^{\infty}\frac{1}{n!}g_{x_0}^{(n)}\sum_{\nu=0}^{n}\binom{n}{\nu}(-x_0)^{n-\nu}M_{\nu} \quad (42)$$

Inserting Equation 42 into Equation 35 gives:

$$\begin{aligned} dC_i/dt = &\frac{1}{2}\sum_{j=1}^{i-1}[K_{rec}(j,i-j)C_jC_{i-j} - (1+\delta_{j,i-j}) \\ &K_{diss}(j,i-j)C_i] \\ &+ \sum_{j=i+1}^{x^*}(1+\delta_{j,i-j})K_{diss}(i,j-i)C_j - \sum_{j=1}^{x^*}K_{rec}(i,j)C_iC_j \\ &+ \sum_{n=0}^{\infty}\frac{1}{n!}K_{diss}^{(n)}(i,\bar{x})\sum_{\nu=0}^{n}\binom{n}{\nu}(-\bar{x})^{n-\nu}\sum_{l=0}^{\nu}\binom{\nu}{l}(-i)^{\nu-l}M_l \\ &- C_i\sum_{n=0}^{\infty}\frac{1}{n!}K_{rec}^{(n)}(i,\bar{x})\sum_{\nu=0}^{n}\binom{n}{\nu}(-\bar{x})^{n-\nu}M_{\nu} + S_i \end{aligned} \quad (43)$$

Also, it is noted that:

$$(x+y)^k - x^k - y^k = \sum_{l=1}^{k-1}\binom{k}{l}y^{k-l}x^l \quad (44)$$

and

$$x^k - y^k - (x-y)^k = \sum_{l=1}^{k-1}\sum_{\lambda=0}^{l}\binom{k}{l}\binom{l}{\lambda}(-1)^{l-\lambda}y^{k-\lambda}x^{\lambda} \quad (45)$$

For $k = 0$, the $(x+y)^k - x^k - y^k$ and the $x^k - y^k - (x-y)^k$ terms reduce to -1 and Equation 39 becomes:

$$\begin{aligned} dM_0/dt = &-\sum_{i=1}^{x^*} dC_i/dt + \sum_{i=1}^{x^*} S_i + \int_{x^*}^{\infty} dx S_x \\ &- \frac{1}{2}\sum_{i=1}^{x^*}\sum_{j=1}^{x^*}[K_{rec}(i,j)C_iC_j] \\ &+ \frac{1}{2}\sum_{j=2}^{x^*}\sum_{i=1}^{j-1}[(1+\delta_{i,j-i})K_{diss}(i,j-i)C_j] \\ &- \sum_{i=1}^{x^*}C_i\sum_{n=0}^{\infty}\frac{1}{n!}K_{rec}^{(n)}(i,\bar{x})\sum_{\nu=0}^{n}\binom{n}{\nu}(-\bar{x})^{n-\nu}M_{\nu} \\ &+ \sum_{i=1}^{x^*-1}\sum_{n=0}^{\infty}\frac{1}{n!}K_{diss}^{(n)}(i,\bar{x})\sum_{\nu=0}^{n}\binom{n}{\nu}(-\bar{x})^{n-\nu}\sum_{l=0}^{\nu}\binom{\nu}{l}(-i)^{\nu-l}M_l \\ &- \frac{1}{2}\sum_{m=0}^{\infty}\sum_{n=0}^{\infty}\frac{1}{m!}\frac{1}{n!}K_{rec}^{(m,n)}(\bar{x},\bar{x}) \\ &\sum_{\mu=0}^{m}\sum_{\nu=0}^{n}\binom{m}{\mu}\binom{m}{\nu}(-\bar{x})^{m+n-\mu-\nu}M_{\mu}M_{\nu} \\ &+ \frac{1}{2}\left[\sum_{m=0}^{\infty}\sum_{n=0}^{\infty}\frac{1}{m!}\frac{1}{n!}K_{diss}^{(m,n)}(\bar{x},\bar{x})\right. \\ &\left.\sum_{\mu=0}^{m}\sum_{\nu=0}^{n}\binom{m}{\mu}\binom{m}{\nu}\bar{x}^{m+n-\mu-\nu}\right] \\ &\times\left[\sum_{l=0}^{\nu}\binom{\nu}{l}\frac{(-1)^{m+n-\mu-l}}{\nu-l+1}\left[M_{\mu+\nu+1} - x*^{\nu-l+1}M_{\mu+1}\right]\right] \end{aligned} \quad (46)$$

For $k = 1$, the $(x+y)^k - x^k - y^k$ and the $x^k - y^k - (x-y)^k$ terms reduce to 0 and Equation 39 becomes:

$$dM_1/dt = -\sum_{i=1}^{x^*} i dC_i/dt + \sum_{i=1}^{x^*} iS_i + \int_{x^*}^{\infty} dx x S_x \quad (47)$$

which, again, is a conservation equation for the number of monomers in the system. For arbitrary k, Equation 39 becomes:

$$\begin{aligned} dM_k/dt = &-\sum_{i=1}^{x^*} i^k dC_i/dt + \sum_{i=1}^{x^*} S_i + \int_{x^*}^{\infty} dx S_x \\ &+ \frac{1}{2}\sum_{i=1}^{x^*}\sum_{j=1}^{x^*}[K_{rec}(i,j)C_iC_j] \times \left[(i+j)^k - i^k - j^k\right] \\ &- \frac{1}{2}\sum_{j=2}^{x^*}\sum_{i=1}^{j-1}[(1+\delta_{i,j-i})K_{diss}(i,j-i)C_j] \\ &\times \left[j^k - i^k - (j-i)^k\right] \end{aligned} \quad (48)$$

$$
\begin{aligned}
&+\sum_{i=1}^{x*} C_i \sum_{l=1}^{k-1}\binom{k}{l} i^{k-l} \sum_{n=0}^{\infty}\frac{1}{n!} K_{rec}^{(0,n)}(i,\bar{x}) \\
&\sum_{\nu=0}^{n}\binom{n}{\nu}(-\bar{x})^{n-\nu} M_{\nu+l} \\
&-\left[\sum_{i=1}^{x*-1}\sum_{l=1}^{k-1}\binom{k}{l} i^{k-l}\sum_{\lambda=0}^{l}\binom{n}{\lambda}(-i)^{l-\lambda}\sum_{n=0}^{\infty}\frac{1}{n!}K_{diss}^{(0,n)}(i,\bar{x})\right] \\
&\times\left[\sum_{\nu=0}^{n}\binom{n}{\nu}(-\bar{x})^{n-\nu}\sum_{\mu=0}^{\nu}\binom{\nu}{\mu}(-i)^{\nu-\mu} M_{\lambda+\mu}\right] \\
&+\left[\frac{1}{2}\sum_{l=1}^{k-1}\binom{k}{l}\sum_{m=0}^{\infty}\sum_{n=0}^{\infty}\frac{1}{m!}\frac{1}{n!}K_{rec}^{(m,n)}(\bar{x},\bar{x})\right] \\
&\times\left[\sum_{\mu=0}^{m}\sum_{\nu=0}^{n}\binom{m}{\mu}\binom{n}{\nu}(-\bar{x})^{m+n-\mu-\nu} M_{\mu+k-l} M_{\nu+l}\right] \\
&-\frac{1}{2}\left[\sum_{l=1}^{k-l}\sum_{\lambda=0}^{l}\binom{k}{l}\binom{l}{\lambda}\sum_{m=0}^{\infty}\sum_{n=0}^{\infty}\frac{1}{m!}\frac{1}{m!}K_{diss}^{(m,n)}(\bar{x},\bar{x})\right] \\
&\times\left[\sum_{\mu=0}^{m}\sum_{\nu=0}^{n}\binom{m}{\mu}\binom{n}{\nu}\bar{x}^{m+n-\mu-\nu}\right] \\
&\times\left[\sum_{\varepsilon=0}^{\nu}(-1)^{l-\lambda+m+n-\mu-\varepsilon}\binom{\nu}{\varepsilon}\frac{1}{k+\nu+1-\lambda-\varepsilon}\right] \\
&\times\left[\left(M_{k+\mu+\nu+1}-x*^{k+\nu+1-\lambda-\varepsilon} M_{\mu+\varepsilon+\lambda}\right)\right]
\end{aligned}
$$

Equations 43 and 48 are two coupled sets of nonlinear ordinary differential equations for the small size cluster concentrations and the continuum moments. If we take only the first two terms in the Taylor series expansion for K_{rec} and K_{diss} into account (i.e., we truncate all terms with m, $n > 2$), then the system is self-contained for any number of moments M_k, $k = 0, 1, \ldots, N$, with $N > 1$. Because the recombination and the dissociation rates are supposed to be smooth functions of size for the large size clusters, this truncation is not considered to be too severe.[27]

3. RESULTS

3.1. Cluster Energetics, Geometry and Normal Modes of Vibrations

The energetics of silicon clusters of up to size 10 atoms and carbon clusters of up to size 10 atoms have been calculated. The calculations were performed using the General Atomic and Molecular Electronic Structure System (GAMESS) Quantum Mechanics software package.[14] Calculations were performed using both ab initio and semi-empirical methods for silicon clusters, and the ab initio method only for carbon clusters. The basis sets used were the TZV[16] basis set for the ab initio calculations and the PM3[17] basis set for the semi-empirical calculations. In this manner, the cluster binding energy, configuration and normal modes of vibration were determined.

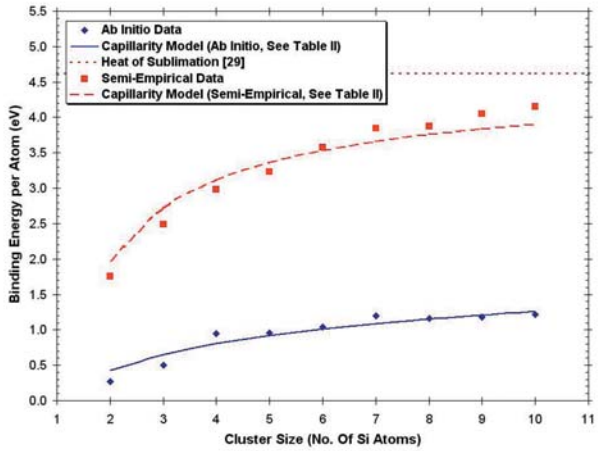

Figure 1. Binding energy per atom for Si as a function of the cluster size using the ab initio and the semi-empirical quantum methods. A capillary model is fitted to the data.

Figure 1 shows the cluster binding energy per atom for silicon clusters as a function of cluster size for both the ab initio and semi-empirical models, and Figure 2 is a similar curve for carbon clusters, but for ab initio calculations only. The data points are the calculated binding energies, and the smooth curves are the binding energies based on the modified capillary model previously discussed. For silicon, the large differences in binding energies between the ab initio model and the semi-empirical model is due to the nature of the semi-empirical calculations, where the lack in rigor is augmented with empirical constants.

A heat of sublimation of 4.619 eV at 0 K[29] was used to determine the bond energies of silicon clusters, and likewise, a heat of sublimation of 7.373 eV at 0 K[29] was used to determine the bond energies of carbon clusters. The power

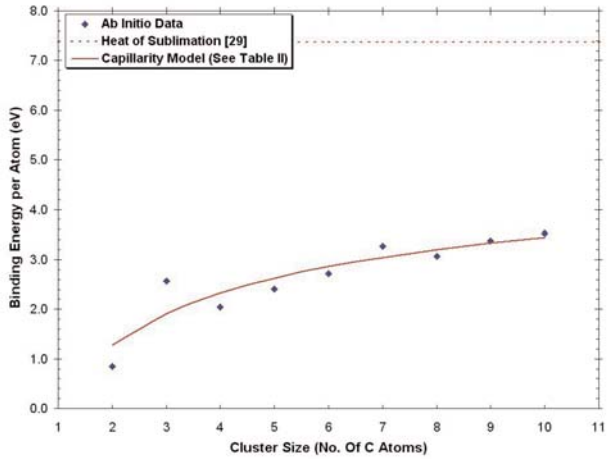

Figure 2. Binding energy per atom for C clusters as a function of the cluster size using the ab initio quantum method. A capillary model is fitted to the data.

Table 2. Modified capillary model coefficients

	Si ab initio	Si semi-empirical	*C*
$\Delta H_{sublimation}$ *(eV)*	4.6190	4.6190	7.3728
m	2.0	2.0	1.5
ϕ *(eV)*	2.3095	2.3095	4.9152
a	0.0	0.0	0.0
α	−0.13852	−0.80837	−0.27375

law coefficients, α, were determined by a least squares fit to the quantuum data. The results are summarized in Table 2. For each case, a best fit was achieved by setting the surface energy parameter, *a*, of Equation 4 to zero. Thus, in effect, Equation 4 becomes:

$$E_{binding} = m\phi x\,(1 - x^{\alpha}) \tag{49}$$

Additionally, the morphology and normal modes of vibration were determined for clusters of up to size 10 silicon atoms and size 10 carbon atoms. These can be found in Ref. 22. Although the bond distances differ somewhat, in general, the semi-empirical model predicts the same cluster geometry as the ab initio model. Also, the semi-empirical model predicts higher frequencies for each mode when compared to the ab initio model. As was previously discussed this is an important consideration when computing thermochemistry or reaction rates.

3.2. Nanocluster Nucleation

In order to study the nanocluster nucleation phenomena, the rate constants developed in section II B were inserted into the master equations developed in section II C. These were coupled to the one-dimensional kinetics (ODK) nozzle expansion equations[22, 30] to study nucleation within a nozzle, and to a well-stirred reactor model to study nucleation in a turbulent environment. The discrete sectional method (section IIC 1) was used to solve the system of equations describing nanocluster nucleation within an expanding gas nozzle, and the moments method (section IIC 2) was used to solve the system of equations describing nanocluster nucleation within a turbulent environment.

3.2.1. Expanding Nozzle Model

The developed model for cluster nucleation in expanding nozzle flow was tested by comparison with experimental data. An earlier experiment was performed at the University of Minnesota in which they produced nanophase silicon.[5] The model was run against the conditions reported in reference 5 and compared to their data. The experiment consisted of using a plasma arc to generate silicon monomers in hot argon at the nozzle entrance. The resultant mixture was then quenched by expanding it through a nozzle. Experimental conditions are given in Table 3. The discrete sectional method was used to solve the coupled ODK/Master Equations for the nozzle. The moments method is not suitable for this problem because it is ill-posed, since the initial conditions for the unknown continuum distribution do not exist.[31] The nozzle conditions are graphically displayed in Figures 3 and 4, where the temperature, pressure and saturation ratio versus nozzle length are shown. The particle size evolution through the nozzle is illustrated in Figure 5. This figure shows that, although some particle size distribution is starting to develop, nucleation and growth of larger size particles do not occur in the nozzle. This is supported by earlier models of the same experiment.[5, 32] As can be seen in Figures 3 and 4, the quench rate is sufficient to produce a rapid increase in saturation ratio (see Figure 4), and the experimental evidence indicates that nucleation is occurring.[5] There must be some other mechanism that is occurring to cause the nucleation. This will be discussed in the next section.

Table 3. Minnesota experiment conditions[5]

	Inlet	Outlet
Diameter (mm)	—	5
Length (mm)	—	50
Pressure (torr)	871	405.6
Temperature (K)	2,400	1,800
N_{Si} (cm^{-3})	10^{14}	6.2×10^{13}
Saturation Ratio	0.024	15
Elapsed Time (μs)	—	95
Velocity (m/s)	—	790.8
Mach No.	—	1.0

3.2.2. Well-Stirred Reactor Model

The reason that nucleation does not occur in the nozzle is that the nucleation rate is so much slower than the nozzle velocity. This situation is very similar to combustion in a jet afterburner. If not for the flame holders, combustion would not occur in the supersonic section of a jet. The reason is that the velocity of the gas stream is greater than the flame speed of the combustion process.[33, 34] Hence, the combustion

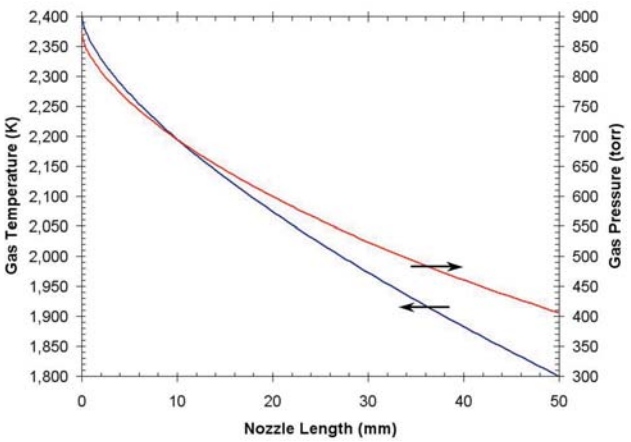

Figure 3. Nozzle temperature and pressure profile.

RESEARCH ARTICLE

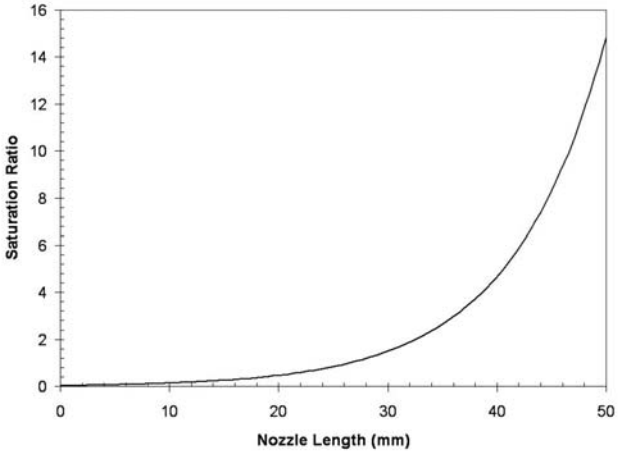

Figure 4. Nozzle saturation ratio profile.

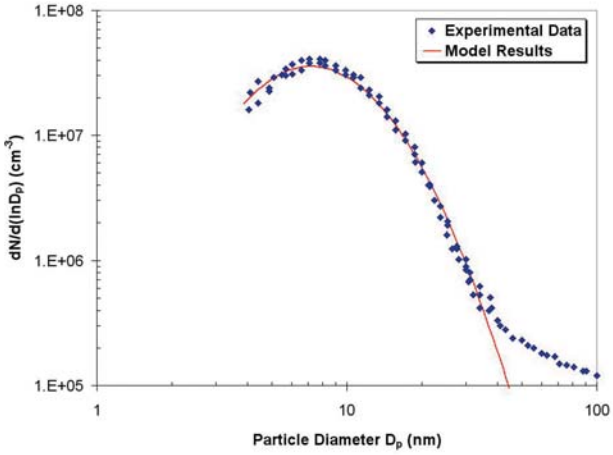

Figure 6. Comparison of model to experiment.[5]

reaction is snuffed-out, similar to blowing out a candle. In order to promote combustion in high velocity streams, flame holders are inserted to stabilize the combustion process. A flame holder consists of either inserting a bluff body in the flow stream or a sudden disruption of the flow stream such as a step or sudden expansion or wall recess, or by secondary gas injection. Flame holders promote strong recirculation zones which stabilize the combustion process. Experiments have shown that combustion is complete within the recirculation zones. The combustion products from the recirculation zone mix with the main flow and ignite it.[33, 34]

A similar process is assumed to take place for the experimental conditions reported in Ref. 5. After the gas is expanded to its final temperature, pressure and supersaturation, it exits the nozzle into a chamber. The interface between the nozzle and the chamber is a large sudden expansion. This sudden expansion causes turbulent recirculation zones to occur. Complete nucleation occurs within the recirculation zones. The complete nucleation products from the recirculation zones mix with the main stream. The nucleation products from the recirculation zones act as nucleation seeds in the main stream and promote nucleation there.

It will be assumed that the nucleation process occurring at the nozzle/chamber interface can be modeled as a well-stirred reactor. The time constant will be determined a posteriori and checked for reasonableness. The results of the model are shown in Figure 6. The resultant time constant, τ, is 2.5 sec. The monomer concentration at the nozzle exit is $4.4 \times 10^{13}\ cm^{-3}$ which compares very well with the results of $6.2 \times 10^{13}\ cm^{-3}$ from the nozzle expansion model and Ref. 5.

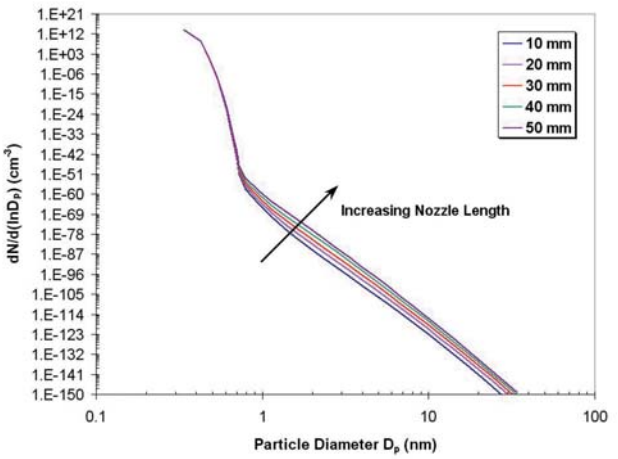

Figure 5. Particle size evolution within nozzle—discrete sectional method.

4. CONCLUSIONS

The work performed here has demonstrated that:

1. Quantum mechanics calculations are needed to accurately determine the characteristics of small size clusters (e.g., shapes, binding energies, vibrational modes, etc.).
2. Small size cluster energetics can be tied to large size cluster energetics by a modified capillary model.
3. QRRK theory predicts the energy transfer limited recombination and dissociation reactions of the small size clusters fairly well. For larger size clusters, where the recombination/dissociation reactions are not energy transfer limited, QRRK reverts to absolute rate theory (also known as transition state theory (TST)).
4. Rates predicted by QRRK and TST are much smaller than rates predicted by collision rate theory.
5. Fissioning of large clusters with one fission fragment larger than 1 atom in size is easily modeled with the methods developed herein. This cannot be easily achieved with collision rate theory.

6. The rate equations coupled to the gas dynamics equations show that nucleation of nanoclusters does not occur in quenching nozzle experiments, such as the experiment reported in Ref. 5. The gas velocity in the nozzle is much greater than the nucleation rate, and most of the particles at the nozzle exit are monomers or dimers.
7. Nucleation occurs outside the nozzle where the gas exits the nozzle into the vacuum chamber.
8. Nucleation is stabilized by the turbulent recirculation zones that are created at the nozzle exit by the sudden expansion.
9. The model developed here predicts the results of the expanding nozzle experiment[5] very well, although the exact geometry of the experimental apparatus and turbulent recirculation zone pattern are not known. Only the nozzle geometry is reported.[5]
10. The turbulent recirculation zone pattern and characteristic time constant determined herein to match experimental results obtained in Ref. 5 are reasonable.

References

1. S. T. Schwab, P. P. Paul, and Y. M. Pan, *Mater. Sci. Eng*. AA204, 197 (**1995**).
2. T. Yamamoto and J. Mazunder, *Nano-struct. Mater*. 7, 305 (**1996**).
3. C. A. Huber, in *Handbook of Nanophase Materials,* edited by A. N. Goldstein, Marcel Dekker Inc., New York, (**1997**), pp. 317–337.
4. D. J. Norris, A. Sacra, C. B. Murray, and M. G. Bawendi, *Phys. Rev. Lett.* E 72, 2612 (**1994**).
5. N. P. Rao, S. Girshick, J. Heberlein, P. McMurry, S. Jones, D. Hansen, and B. Micheel, *Plasma Chem. Plasma Processing* 15, 581 (**1995**).
6. P. W. Atkins, *Physical Chemistry, W.* H. Freeman and Co., New York (**1982**), 2nd ed.
7. J. H. Seinfeld and S. N. Pandis, *Atmospheric Chemistry and Physics; From Air Pollution to Climate Change* John Wiley & Sons, Inc., New York (**1998**).
8. G. D. Stucky, *Naval Res*. Rev. 3, 28 (**1991**).
9. S. M. Senkan, in *Advances in Chemical Engineering* Academic Press, Inc., San Diego (**1992**), vol. 18, pp. 95–196.
10. S. Glasstone, K. J. Laidler, and H. Eyring, *The Theory of Rate Processes,* McGraw-Hill Book Company, Inc., New York (**1941**).
11. R. D. Present, *Kinetic Theory of Gases* McGraw-Hill Book Co., (**1958**).
12. J. P. Lowe, *Quantum Chemistry* Academic Press, San Diego (**1993**), 2nd ed.
13. D. A. Park, *Introduction to the Quantum Theory,* McGraw-Hill Book Co., New York (**1964**).
14. M. W. Schmidt, K. K. Baldridge, J. A. Boatz, S. T. Elbert, M. S. Gordon, J. J. Jensen, S. Koseki, N. Matsunaga, K. A. Nguyen, S. Su, et al., *J. Comput. Chem.* 14, 1347 (**1963**).
15. J. A. Pople and D. Beveridge, *Approximate Molecular Orbital Theory,* McGraw-Hill Book Co., New York (**1970**).
16. A. D. McLean and G. S. Chandler, *J. Chem. Phys*. 72, 5639 (**1980**).
17. J. J. P. Stewart, *J. Comput. Chem*. 10, 209 (**1989**).
18. L. S. Kassel, *The Kinetics of Homogeneous Gas Reactions,* The Chemical Catalog Company, Inc. (**1932**).
19. L. S. Kassel, *J. Phys. Chem*. 32, 1065 (**1928**).
20. J. Gardiner, and J. Troe, in *Combustion Chemistry,* edited by J. W. C. Gardiner Springer-Verlag, Berlin, (**1984**), pp. 173–196.
21. M. R. Lindeburg, *Mechanical Engineering Review Manual* Professional Publications (**1984**), 7th ed.
22. G. A. Johnson, Ph.D. thesis, University of California, Los Angeles (**2003**).
23. N. Ashcroft and N. Mermin, *Solid State Physics,* Holt, Rinehart, and Winston, New York (**1976**).
24. R. H. Perry and C. H. Chilton, eds., *Chemical Engineers' Handbook* McGraw-Hill Book Co., New York (**1973**), 5th ed.
25. R. L. Rowley, *Statistical Mechanics for Thermophysical Property Calculations,* Prentice-Hall, Englewood Cliffs, NJ (**1994**).
26. F. Gelbard, Y. Tambour, and J. H. Seinfeld, *J. Colloid Interface Sci.* 76, 541 (**1980**).
27. M. Vicanek and N. M. Ghoniem, *J. Comput. Phys*. 101 (**1992**).
28. R. L. Drake, in *Topics in Current Aerosol Research,* edited by G. M. Hidy and J. R. Brook, Pergamon, Oxford (**1972**), vol. 3, p. 201.
29. R. C. Weast, ed., *CRC Handbook of Chemistry and Physics* CRC Press, Boca Raton, FL (**1981**), 61st ed.
30. A. H. Shapiro, *The Dynamics and Thermodynamics of Compressible Fluid Flow,* The Ronald Press Co. (**1953**).
31. C. A. Stone, Ph.D. thesis, University of California, Los Angeles (**1990**).
32. Q. Wei, Master's thesis, University of Minnesota (**1994**).
33. I. Glassman, *Combustion,* Academic Press, Inc., San Diego(**1987**), 2nd ed.
34. G. C. Oates, *Aerothermodynamics of Aircraft Engine Components,* AIAA, Inc. (**1985**).

Received: 16 October 2003. Revised/Accepted: 5 November 2003.